

1 **More dynamic than expected: An updated survey of surging glaciers** 2 **in the Pamir**

3 Franz Goerlich¹, Tobias Bolch², Frank Paul¹

4 ¹Department of Geography, University of Zurich, Zurich, Switzerland

5 ²School of Geography and Sustainable Development, University of St. Andrews, St. Andrews, United Kingdom

6 *Correspondence to:* Franz Goerlich (franz.goerlich@geo.uzh.ch)

7 **Abstract.** The investigation of surging glaciers using remote sensing has recently seen a strong increase as freely
8 available satellite data and digital elevation models (DEMs) can provide detailed information about surges that
9 often take place in remote and inaccessible regions. Apart from analysing individual surges, satellite information
10 is increasingly used to collect valuable data on surging glaciers. Related inventories have recently been published
11 for several regions in High Mountain Asia including the Karakoram, parts of the Pamir and western Kunlun
12 Shan, but information for the entire Pamir is solely available from a historic database listing about 80 glaciers
13 with confirmed surges. Here we present an updated inventory of confirmed glacier surges for the Pamir that
14 considers results from earlier studies and is largely based on a systematic analysis of Landsat image time series
15 (1988 to 2018), very high-resolution imagery (Corona, Hexagon, Bing Maps, Google Earth) and DEM
16 differences. Actively surging glaciers were identified from animations and flicker images (e.g. terminus
17 advances) and the typical elevation change patterns (lowering in an upper reservoir zone and thickening further
18 down in a receiving zone). In total, we identified 206 spatially distinct surges within 186 glacier bodies, mostly
19 clustered in the northern and central part of the Pamir. Where possible, minimum and maximum glacier extents
20 were digitized, but often interacting tributaries made a clear separation challenging. Most surging glaciers (n=70)
21 are found in the larger size classes (>10 km²), but two of them are very small (<0.5 km²). We found also several
22 surges where the length of the glacier increased by more than 100%. The created datasets are available at:
23 <https://doi.pangaea.de/10.1594/PANGAEA.914150> (Goerlich et al., 2020).

24

25 **1 Introduction**

26 The investigation of surging glaciers using satellite data has recently received increased attention among
27 scientists, in particular for the Karakoram mountain range but also other regions of the world (e.g. Berthier and
28 Brun, 2019; Bhambri et al., 2017; Bolch et al., 2017; Falaschi et al., 2018; Minora et al., 2016; Paul, 2015 and
29 2020; Quincey et al., 2015; Rankl and Braun, 2016; Round et al., 2017; Steiner et al., 2018). This has several
30 reasons, for example (a) the free access to long (Landsat) and dense (TerraSAR-X / TanDEM-X, Sentinel-1/2)
31 time series of high-resolution satellite data, (b) the limited understanding of why some glaciers in this region are
32 surging while others do not, (c) a large number of on-going surges at any point in time, (d) the large variations of
33 surge behaviour in a small region, (e) the long history of still occurring surge-related hazards (mostly due to
34 damming of a river and related outburst of lakes), and (f) the very difficult field access. Thereby, most studies
35 document the variations in glacier extent / length changes, flow velocities and elevation / mass changes in the

36 course of a surge or surge-related hazards. These studies have revealed unprecedented details about surge
37 dynamics and variations that have already helped in improving our understanding of related surge mechanisms.

38

39 In contrast, the surging glaciers in the Pamir mountain ranges to the north of the Karakoram received less
40 attention, but recently some studies were published (e.g. Lv et al. 2019; Osipova 2015; Wendt et al. 2017; Holzer
41 et al. 2016). This might be due to the fact that several surges during the Soviet era have already been described in
42 detail (e.g. the surges of Medvezhy and Geographical Society glaciers are well documented, see Dolgushin and
43 Osipova (1971, 1975), Kotlyakov et al. (2003) and Osipova (2015)) and a detailed inventory describing a high
44 number (>800) of surge-type glaciers based on satellite data and aerial images was published (Osipova et al.
45 1998). However, this and many of the publications are in Russian and are therefore little known internationally.

46

47 When speaking about surging glaciers, we first have to differentiate between surge-type glaciers and other
48 glaciers. This is important when interpreting glacier changes in the context of climate change, e.g. their length or
49 mass changes over a time period when surges have occurred (Bolch et al., 2017; Brun et al., 2017; Gardelle et al.,
50 2013). Secondly, it is also important to distinguish surge-type from surging glaciers. The former have surged at
51 some point in the past and show indirect evidence like looped or distorted moraines or post-surge down-wasting
52 features of a former surge, whereas the latter surged actively within the observation period. Looped or otherwise
53 distorted moraines occur due to former surges that pushed the lobate-shaped boundaries of tributaries down
54 glacier, indicating different flow speeds among major, moraine-separated glacier branches (Herreid and Truffer,
55 2016; Meier and Post, 1969). The typical post-surge down-wasting features consist of separated lower glacier
56 parts and/or the jagged boundary of a stagnant and rapidly lowering glacier tongue, among others (Paul, 2020).
57 We here only investigate glaciers that have actively surged during the observation period. The globally most
58 complete compilation of surge-type glaciers by Sevestre and Benn (2015) is a valuable starting point, but it is
59 based on literature sources up to the year 2013 only. In the meantime, numerous other surge-type glaciers have
60 been identified across High Mountain Asia (HMA) from the analysis of multi-temporal satellite imagery, e.g. in
61 the Karakoram (Bhambri et al., 2017), Kunlun Shan (Yasuda and Furuya, 2015), central Tibet (Zhang et al.,
62 2018), eastern Pamir (Lv et al., 2019) and Tian Shan (Mukherjee et al., 2017), but an update of confirmed surges
63 for the entire Pamir Mountains is yet missing. With this study we aim to identify them and provide detailed
64 information (e.g. timing and typology) about confirmed glacier surges in the Pamir Mountains.

65

66 Surge-type glaciers in the Pamir are included in the inventory by Osipova et al. (1998) and Sevestre and Benn
67 (2015). There are thus important differences in our approach compared to the methodology used for the
68 ‘catalogue’ by Osipova et al. (1998), implying that both are not directly comparable: (i) our satellite image time
69 series (Landsat) has a lower spatial resolution (30 m) than the KFA1000 data (3-5 m) used by Osipova et al.
70 (1998), (cf. also Dowdeswell et al. 1993, 1995), (ii) we cover a different period (1988–2018) than Osipova
71 (1998), (iii) we have used different indicators for surge identification (e.g. animations, DEM difference patterns),
72 (iv) we have assigned only one surge class instead of six and (v) our glacier entities have different boundaries as
73 we used the most recent Pamir glacier inventory by Mölg et al. (2018) as a base for the analysis (here named GI-
74 1).

75

76 The information from Osipova et al. (1998) is also available in the Randolph Glacier Inventory (RGI) version 6
77 (RGI Consortium 2017) using the simplified classification scheme developed by Sevestre and Benn (2015). We
78 have used the RGI dataset and revisited existing literature, e.g. the study by Lv et al. (2019), as a starting point
79 for our inventory of glacier surges. Our analysis is primarily based on animated multi-temporal (1988-2018)
80 time-series of Landsat data, but also on elevation difference maps showing the typical mass transfer pattern of
81 glacier surges. For some less clear cases, we also analysed very high-resolution images from the Corona and
82 Hexagon missions and the images in Google Earth and Bing Maps for confirmation.

83

84 For this study, we revisited the GI-1 inventory by adding ice divides for glacier units that surged but were so far
85 still connected with other glaciers in GI-1, resulting in a new inventory GI-2. In a second step, three inventory
86 subsets are created from GI-2 that provide (a) the selection of surging glaciers only (GI-3), (b) minimum (GI-
87 3min), and (c) maximum (GI-3max) extents of all surging glaciers. In the following, the number in brackets after
88 a glacier's name refers to its ID in the GI-3min inventory. We also present a rough classification of the different
89 surge-types, the timing of surges during the observation period (1988-2018), a comparison of geomorphometric
90 characteristics (other glaciers in GI-2 vs. GI-3), and a description of geometric changes due to a surge.

91 **2 Study region**

92 The Pamir is one of highest mountain ranges within HMA and of the world extending from about 36°35' to
93 39°35' N and 70°35' to 75°35' E (Fig. 1). The northern part belongs to the Osh region of Kyrgyzstan, the eastern
94 parts to the Xinjiang Uighur Autonomous Region of China, the most southern regions to Badakhshan in
95 northeastern Afghanistan and the main part to Gorno-Badakhshan in Tajikistan. The highest peak (Mt. Kongur)
96 reaches up to 7649 m a.s.l. and enthrones over the Kongur Shan in the eastern part of the Pamir. Here and in the
97 following we use names from transliterated Russian topographic maps at a 1:500.000 scale (see Table S1 in the
98 Supplement).

99

100 *Figure 1*

101

102 Typical glaciers in the Pamir are long and dendritic or multi-basin valley glaciers, but other types such as
103 mountain glaciers and cirques exist as well. Due to the steep and ice-free surrounding rock walls, most glaciers
104 are at least partly debris covered, which often simplifies the identification of typical surge marks (e.g. looped
105 moraines) from space (e.g. Kotlyakov et al. 2008). Most glaciers are concentrated in the central part around
106 Ismoil Somoni Peak (7495 m a.s.l.) including Fedchenko Glacier, which is with a length of >70 km the longest
107 valley glacier in the world outside the polar regions (Machguth and Huss, 2014). Additionally, the region is home
108 to abundant rock glaciers that are not always clearly separable from debris-covered glaciers and other ice-debris
109 landforms (Mölg et al., 2018).

110

111 The glaciers in the western and central part of the Pamir (Tadjik, Kyrgyz and Afghan regions) are of winter
112 accumulation type where most precipitation (~90%) falls between December and May (Maussion et al., 2014)
113 with annual amounts of up to 1285 mm a⁻¹ at Fedchenko weather station at 4169 m.a.s.l. (Finaev et al., 2016).
114 Conversely, the glaciers in the eastern part are mainly (50 to 60%) fed by precipitation in the summer months
115 between June and August, which can be seen as an effect of the monsoon (Maussion et al., 2014). The total
116 annual precipitation is very low in some regions, reaching only ~70 mm a⁻¹ at Murgab (3576 m a.s.l.) and
117 Toxkargan (3090 m a.s.l.) weather stations, both located in valleys (Finaev et al., 2016). Hence, the glaciers in
118 the western and central part are situated in a somewhat warmer and more humid climate whereas the eastern
119 ranges are dry and cold. Accordingly, glacier mean elevations of the former can be found at lower altitudes
120 (~4740 m a.s.l.) than in the eastern regions (~5050 m a.s.l.) according to the dataset presented by Mölg et al.
121 (2018).

122

123 The likely best-investigated glacier in the region is Fedchenko (Lambrecht et al., 2014, 2018) that is so far
124 considered as not of surge-type. Of the glaciers with confirmed surges, Medvezhy Glacier (29, ObjectID in the
125 GI3-min inventory) is likely the best investigated (see Kotlyakov et al., 2008). This latter study also reported
126 details about surges of several other glaciers in the region, partly back to 1959.

127 **3 Datasets and pre-processing**

128 **3.1 Satellite data**

129 **3.1.1 Landsat**

130 For the detection of glacier surges and determination of surge start, end and possibly their full surge cycle (e.g.
131 from the starting year of an active phase to the start of the next active phase), we used freely available Landsat
132 imagery (Level 1T) from earthexplorer.usgs.gov including Landsat 5 TM (Thematic Mapper), Landsat 7 ETM+
133 (Enhanced Thematic Mapper plus) and Landsat 8 OLI (Operational Land Imager) sensors. Additionally, we used
134 some very good scenes (no snow outside glaciers) from Landsat MSS (Multispectral Scanner) from the 1970s
135 and 1980s. The three sensors TM, ETM+ and OLI acquire data with a horizontal resolution of 30 m for the
136 visible, near-infrared (NIR) and shortwave infrared (SWIR) bands at a repeat rate of 16 days. Key characteristics
137 of the datasets are shown in Table 1; the full list of scenes used for this study is presented in Table S2 in the
138 Supplementary Material.

139

140 In general, cloud-free scenes from the end of the summer (July to October) are used from all sensors, but for
141 some regions, also earlier acquisitions are considered to have images available for as many years as possible.
142 With a focus on the changes near the glacier terminus, the remaining seasonal snow at higher elevations in these
143 images was unproblematic. Unfortunately, it was not possible to find suitable scenes for each year in most
144 regions so that the determination of the onset or end of a surge has at least a ± 1 year uncertainty. Priority was
145 given to Landsat 5 TM scenes to limit using Landsat 7 ETM+ scenes after 2002 when the Scan Line Corrector
146 (SLC) stopped working (resulting in so-called SLC-off scenes). For the animations we downloaded the standard
147 colour-balanced and orthorectified image quicklooks from earthexplorer.usgs.gov that are provided in false-

148 colours (glacier ice and snow is depicted in cyan) and at the original resolution. The jpg-compression of these
149 images results locally in blurred details but they had only a very small impact on surge identification.

150

151 *Table 1*

152

153 **3.1.2 Corona and Hexagon**

154 The Corona Keyhole (KH) 4B scenes from August 1968 (Table S1) cover the central and northern Pamir (see
155 Fig. 1) and were also downloaded from earthexplorer.usgs.gov. The Corona images are panchromatic, recorded
156 in stereo mode and have a ground resolution of up to 1.8 m (Galiatsatos, 2009). We processed 11 scene pairs to
157 generate a DEM and corresponding orthophotos with 5 m resolution following Goerlich et al. (2017). Due to the
158 high effort of processing the scenes, the orthoimages only cover the region with the most surging glaciers. The
159 orthoimages revealed details in surface morphology that are typical for surging glaciers but barely visible for the
160 largest glaciers at the 30 or 15 m resolution of Landsat images. We also used Hexagon KH-9 scenes from July
161 1975 and June 1980 to generate orthoimages following Pieczonka et al. (2013). The scenes depict the regions
162 west of lake Karakul with a resolution of up to 6 m.

163 **3.1.3 Google Earth and Bing Maps**

164 The very high-resolution (a few m or better) satellite images available in Google Earth (GE) have been widely
165 used for numerous geoscientific applications (Liang et al., 2018). We used them here together with the satellite
166 images available on Bing Maps to confirm identified surging glaciers in the Landsat period, i.e. for visual checks
167 only. Sometimes the available time series in GE also allowed a proper identification of glacier surges when the
168 quiescent and/or active phases are captured (see examples in Lv et al., 2019). Interestingly, the images used in
169 Bing Maps were often complimentary to GE, i.e. provided excellent coverage when nothing useful was available
170 in GE and vice versa.

171

172 In Fig. 2 we provide a visual comparison of image sources displaying three surging glaciers in the central Pamir
173 to illustrate the visibility of details. We include examples from Corona, Hexagon, Landsat OLI as well as GeoEye
174 (from Bing Maps). The high-resolution images from Corona and Bing Maps clearly show the highly crevassed
175 surfaces (mainly for the two larger glaciers) that are not visible in the Landsat image. In the Landsat image, the
176 glacier boundary and debris-covered parts can be identified, but it is almost impossible to reveal the terminus of
177 Walter 731 (19) and Soldatov (20) glaciers in the static image. This is different when using animations that reveal
178 glacier termini clearly when they change position (Paul, 2015).

179

180 *Figure 2*

181

182 **3.2 Digital elevation models (DEMs)**

183 Several DEMs are freely available for the study region. This includes the Shuttle Radar Topography Mission
184 (SRTM) DEM (Rabus et al., 2003), the Advanced Spaceborne Thermal Emission and Reflection Radiometer
185 (ASTER) GDEMv3 (NASA, 2018), the ALOS PRISM DEM AW3D30 (Takaku et al., 2014), the High Mountain
186 Asia (HMA) DEM (Shean, 2017) and the DEM from the TanDEM-X mission (TDX) provided by DLR (German
187 Aerospace Centre) (Wessel, 2016). They have different characteristics (sensor types, spatial resolution, artefacts,
188 data voids, acquisition dates) and – apart from the HMA DEM – are used here for several purposes such as
189 calculation of topographic characteristics and surface elevation changes (Table 2). A direct comparison of the
190 DEMs using hillshades and DEM differences revealed that only the GDEMv3 and the AW3D30 DEM are free of
191 data voids but that the AW3D30 has some artefacts over glacier surfaces and too high elevations. We thus used
192 the GDEMv3 to determine topographic characteristics for all glaciers.

193

194 Besides the orthoimages, we created DEMs from the 1968 Corona stereo pairs (cf. Goerlich et al., 2017) and used
195 DEMs from 1975 Hexagon data (cf. Pieczonka et al., 2013). The AW3D30 DEM served as a height reference
196 (Ground Control Points, Disparity Predictions) for the Corona DEM processing and the SRTM DEM for
197 Hexagon. The main difference of the final DEMs is the coverage where Corona covers only a small area (~15 km
198 x 180 km) per stereo image pair compared to Hexagon (~130 km x 130 km). This results in a far larger effort to
199 generate DEMs and orthophotos from Corona for a larger region.

200

201 We have used the temporally better constrained DEMs from Corona (1968), SRTM (2000), AW3D30 (2006-
202 2011), and TDX (2011-2014) to determine elevation changes over the periods of 1968 to 2000, 2000 to ~2009,
203 and ~2009 to ~2012/14. Elevation differences were interpreted in a qualitative sense only as the typical pattern of
204 elevation changes for surging glaciers (strong elevation gain in the lower and loss in the upper region during the
205 active phase of a surge, and vice versa for the quiescent phase) can be clearly identified in most cases, i.e.
206 changes are often much higher (100+ m) than the combined uncertainties of the two DEMs (e.g. Gardelle et al.
207 2013).

208

209 *Table 2*

210

211 **3.3 Glacier outline datasets**

212 We used the Karakoram / Pamir glacier inventory (GI-1) created by Mölg et al. (2018) as a basis for glacier
213 identification and extent modification. This inventory provides a consistent dataset of manually corrected glacier
214 outlines based on Landsat scenes acquired between 1998 and 2002 for the entire Pamir, including the ranges
215 Kingtau, Ulugarttag and Muztagh in the Chinese part (see Fig. 1). As the inventory is a temporal snap shot and
216 surge-type glaciers are in various stages of their surge cycle, they can be connected to a larger main glacier and
217 thus not be analysed separately. To overcome this restriction, we have separated all part-time tributaries
218 exhibiting their own dynamics from the glaciers they connect with and added the required new ice divides in the
219 accumulation regions. This revised inventory (GI-2) is used as the base for all subsequent geomorphometric

220 calculations. The separation follows the natural flow and extent of the larger glacier and required several
221 iterations of adjustments, as the surge characteristics were often not clear from the beginning. After all surges
222 have been identified, a sub-sample of GI-2 was created that only includes the glaciers that surged (inventory GI-
223 3). The GI-3 sub-sample served as a base to digitise minimum and maximum glacier extents for all glaciers
224 exhibiting a visible change in terminus position. These datasets are saved in two additional inventories (GI-3min
225 and GI-3max, respectively).

226 **4. Methods**

227 **4.1 Surge identification**

228 Glacier surges can occur in very different forms with a likely continuous transition between unstable flow and
229 regular glacier advances. Hence, a clear identification of surge-type glaciers is not trivial even in their active
230 phase and a wide range of identification criteria has been suggested to distinguish them from all other glaciers
231 (e.g. Sevestre et al., 2015; Bhambri et al., 2017; Mukherjee et al., 2017). In this study, we focus on glaciers that
232 had an active surge phase during the investigated period 1988-2018, i.e. indirect evidences alone such as distorted
233 or looped moraines are not considered. Consequently, our sample is smaller than the one presented in the
234 ‘catalogue’ by Osipova et al. (1998), who listed 845 surge-type glaciers for the Pamir (i.e. 35% of the global
235 sample by Sevestre and Benn (2015)) in six distinct classes. Their inventory is also digitally available in the RGI
236 using the simplified classification scheme by Sevestre and Benn (2015), with the classes (their Table 4):
237 confirmed (Category 3), probable (2) and possible (1). With our focus on observed surges (with few exceptions)
238 our sample would be in the ‘confirmed’ type of which Osipova et al. (1998) list 61 and Sevestre and Benn (2015)
239 90 glaciers.

240

241 To identify surging glaciers, we started with the ‘confirmed’ samples listed by Osipova et al. (1998, 2010),
242 Kotlyakov et al. (2008) and Lv et al. (2019). These studies included all mountain ranges where we searched for
243 surging glaciers except the Rushanskii and Muztagh ranges. Our identification consists of four steps:

244

245 (I) At first, we analysed animations from the Landsat quicklooks to validate the findings of the four studies. Each
246 frame set was animated with slightly different samples (varying selection of animated scenes within one frame
247 set) to facilitate visibility of glacier dynamics in each region similar to Paul (2015). The qualitative analysis
248 tracked surface feature displacements and was applied to the entire study region. Collectively, this step revealed
249 139 surging glaciers during the period 1988-2018 (including glaciers that have just started surging).

250 (II) In the next step, we analysed the elevation change patterns of the various DEM difference maps in a
251 qualitative way (Mukherjee et al., 2017). Glaciers showing the typical opposing pattern of surface elevation
252 change along the glacier flowline (lowering and thickening) were digitally marked and added to the sample,
253 yielding 35 further glaciers from the 1968 to 2000 and 2000 to c. 2009 elevation difference maps. For this
254 analysis it does not matter in which region of a glacier the pattern occurs (e.g. internal surges may appear higher
255 up and do not reach the terminus). Two examples of the related DEM difference maps are displayed in Fig. 3,

256 revealing for some glaciers the typical surge pattern. This method helped in detecting internal surges with limited
257 or no changes of the terminus position and/or where crevasses or shear margins are difficult to detect.

258

259 *Figure 3*

260

261 (III) In this step, we analysed individual image pairs in detail using flicker images, i.e. going back and forth
262 between two images only (Kääb et al. 2003). For a clear before/after distinction, this analysis was restricted to the
263 best scenes available for a specific region (e.g. without clouds, seasonal snow or deep shadows). We here also
264 used the contrast-enhanced false colour infrared images from the MSS scenes, several 15 m panchromatic images
265 of ETM+ and OLI and the declassified orthoimages. An additional 27 surging glaciers could be identified this
266 way.

267

268 (IV) In the final step, we checked the identified glaciers with the partially very high-resolution images available
269 in GE and Bing Maps to also analyse morphological characteristics of the glacier surfaces in detail, their shape
270 and also possible changes in extent (Lv et al., 2019). Despite the variability in acquisition years, this allowed us
271 to remove a few glaciers (7) from the sample (in most cases the ‘surges’ were likely just advances) and also add
272 12 new ones. We classified a glacier advance as when the glacier does not show any of the typical surface
273 features such as a heavily crevassed surface, shear margins or collapsing/down-wasting patterns at the tongue and
274 a comparably small and/or slow advance. At this stage, we started introducing indirect evidence (surface features)
275 to the classification and thus checked back if the (mostly small) glaciers have really surged using animations. In
276 some cases it was necessary to interpret results from steps (I) to (III) collectively for a reasonable result.

277

278 Based on the created inventory subset with surging glaciers only (GI-3), we digitised the minimum (GI-3min)
279 and maximum (GI-3max) extent of all glaciers based on the satellite images described in Section 3.1. For glaciers
280 with more than one surge, the respectively largest and smallest extents were digitised (Fig. 4). Whereas
281 maximum extents are in most cases well identifiable, outlines for GI-3min can have larger uncertainties due to
282 the difficulties in clearly identifying the new terminus among the often debris-covered and down-wasting ice
283 from the previous surge. Ideally, the minimum extent is identified once the next surge has started, but for many
284 glaciers this did not happen during the observation period.

285

286 *Figure 4*

287

288 **4.2 Surge characteristics and classification**

289 There are a wide range of possibilities to characterise surges as they have a high variability of appearance and
290 dynamics (e.g. Bhambri et al. 2017). For the GI-3min inventory we have determined a series of key surge
291 characteristics in the attribute table (e.g. surge start / end / duration, and distance) and a simplified classification
292 according to a pre-defined criteria set for statistical analysis and comparison with other regions. It has to be noted
293 that a precise start/end year was often difficult to determine either due to missing satellite data, but also when

294 surge initiation is related to a mass wave coming down from higher elevations (taking a few years) or when
295 remaining dead ice from a previous surge was reactivated. We here defined the start of a surge as the year when
296 an advance of the terminus or a mass wave higher up the glacier (as not all surges show a terminus advance) is
297 detectable. The end of the active phase (maximum extent) is reached when all surge dynamics settle and the
298 quiescent phase begins. The surge duration is calculated by subtracting the start year from the end year of the
299 surge. The latter was easier to determine than minimum extents in most cases.

300

301 To illustrate a few of the possible surge types and interactions, Fig. 5 displays a sketch map of three glaciers that
302 are all surging at some stage. Starting with a surge of the permanently connected tributary (2) in Fig. 5a, this
303 surge is at its maximum extent in Fig. 5b and the ice from the surge is already slightly moved downstream by the
304 flow of the main glacier (1). In addition, glacier (3) started surging in the meantime, connects to the main glacier
305 in Fig. 5b and enters glacier (1) in Fig. 5c where it also reaches its maximum extent. Some time later (Fig. 5d),
306 also the main glacier (1) is in full surge mode and transports the surge marks of both tributary surges
307 downstream, stretching and possibly deforming them. This illustrates the variety of surge interactions (by far not
308 all) and the difficulty to define maximum extents of tributary glaciers. Their surge marks are moved downstream
309 by the main glacier during or near the end of their own surge due to its normal flow or a surge of the main
310 glacier. Accordingly, there is also some uncertainty in the timing of the surge end for glaciers (2) and (3). In this
311 case the main glacier body (1) would have listed two surges in the attribute table of GI-3min and would have
312 been selected to receive the surging classification code.

313

314 *Figure 5*

315

316 For the classification scheme, we used the following criteria and values for each glacier:

317 (A) 'surging?': no = 0, yes = 1, if yes:

318 (B) glacier tongue: free end = 1, connects to another glacier = 2, tributary = 3

319 (C) type of surge: advancing = 1, internal = 2, combined = 3

320 (D) active phase duration: 1-3 years = 1, 4-10 years = 2, >10 years = 3

321 (E) terminus advance: none = 0, short (<1 km) = 1, medium (1-2.5 km) = 2, long (> 2.5 km) = 3.

322 In (C), the 'advancing' type defines a glacier that has a visible terminus change, 'internal' has no advance but
323 either a visible mass wave in the Landsat images or in the DEM difference images. The combined type describes
324 glaciers that show a mass wave within the glacier reaching the terminus and pushing it further down valley.

325 Hence, the entry in the attribute table of GI-2 is either 0 or 1 and stored in a separate 'surge' column. The
326 resulting code from our classification in GI-3min is then for example 2123. This means that the glacier is
327 connected to another glacier during its surge, that it has an advancing tongue and surged over a period of 4-10
328 years over a long distance. In the case the glacier already surged in 1988 or was still surging in 2018, these two
329 years were used as the start or end date. Such dates indicate that the real surge duration is likely longer than given
330 in the table.

331 **4.3 Topographic and other information**

332 For all glaciers in GI-2, we calculated the following attributes according to Paul et al. (2002, 2009): centre point
333 latitude and longitude, area in km², minimum, maximum, mean, and median elevation, mean slope and aspect,
334 and aspect sector. Mean values are calculated as the arithmetic average of all DEM cells covered by the
335 respective glacier. All attributes are also transferred to GI-3, and additionally calculated for GI-3min and GI-
336 3max. The attributes of GI-2/GI-3 depict the glacier state around the year 2000. For GI-3min/GI-3max the
337 attribute date varies between 1988 and 2018 due to the minimum and maximum extent of the glaciers. All
338 elevation dependent attributes are based on ASTER GDEMv3 elevations.

339 **5. Results**

340 **5.1 Distribution and topographic characteristics of surge and other glaciers**

341 From the ~13500 glaciers in the study region, 186 have been identified as surging glaciers of which 206 spatially
342 distinct surges have been identified between 1988 and 2018. Their occurrence is clustered in the central, northern
343 (central and western Pamir Alai, Fedchenko and ‘Petr Alervogo East’) and eastern ranges (Muztagh and
344 Ulugarttag) (Fig. 6). This pattern shows a large gap of glacier surges around Lake Karakul and to the south of the
345 study region with few exceptions. Overall, these latter regions are dominated by comparably smaller glaciers and
346 drier climate, indicating that there might be a size and climatic threshold for surge activity as suggested by
347 Sevestre and Benn (2015).

348

349 *Figure 6*

350

351 The 186 surging glaciers cover a total area of ~2670 km² (with ~110 km² variability due to the surges). Eight of
352 them (~5%) are smaller than 1 km² covering an area of ~7 km², whereas 38% are larger than 10 km² covering an
353 area of 2170 km² (or 81%) (Table 3). Garmo Glacier main trunk (80) is the largest surging glacier (83 km²) and
354 the largest non-surging glacier is Fedchenko. It is a huge dendritic valley glacier with a size of ~580 km² (without
355 the surging Bivachny tributary) and is covering 6% of the total glacier area. The region is thus dominated by the
356 vast size of Fedchenko Glacier with impacts on size-related distributions.

357

358 *Table 3*

359 The created inventories have a different count of entries due to different glacier states and topologic relations.
360 The generalised statistics for the sample with observed surges refer to the GI-3 inventory with 186 entries, whilst
361 statistics for GI-3min and GI-3max have different numbers. Compared to the full sample of glaciers in GI-2
362 (13495), surging glaciers constitute 77% by number and 80% by area in the area class 50-100 km² (Fig. 7). They
363 are also dominating the size classes 10-50 and 100-500 km² (51% and 63% by area, respectively). When
364 considering all three size classes from 10 to 500 km², two thirds of the glaciers have surged in the observation
365 period, i.e. they are the rule rather than the exception. The 22 largest surging glaciers cover about the same area
366 (1338 km²) as the 163 smaller ones (1332 km²).

367

368 *Figure 7*

369

370 The frequency distribution of aspect sectors of surging glaciers is only slightly different from all other glaciers
371 (Fig. 8a). Surging glaciers exposed to SW contribute almost 10% of the sample, whereas only 3% of the other
372 glaciers are facing in this direction. The same applies to the area covered (Fig. 8b), where surging glaciers
373 cumulate ~370 km² and thus ¼ more area than the other glaciers (~300 km²) in this sector. On the other hand, the
374 latter have higher percentages facing N and NE. The strong difference towards the N is mainly driven by
375 Fedchenko Glacier.

376

377 *Figure 8*

378

379 The scatter plot showing median elevation vs. mean aspect (Fig. 9) reveals that median elevations cover a wide
380 range of values (from about 3500 to 6000 m) and that there is some dependence on aspect, i.e. glaciers facing
381 south have a few hundred metres higher median elevations. The surging glaciers largely follow this distribution,
382 but have somewhat higher elevations in the southern and lower values in the northern aspect ranges compared to
383 the other glaciers when considering median values per sector. On average, the median elevation of surging
384 glaciers is 4800 m a.s.l.

385

386 *Figure 9*

387

388 Median glacier elevations increase from west to east and show a small decrease in the most eastern and northern
389 ranges (Pamir Alai) towards the outer glaciers (Fig. 10). The marked surging glaciers are mostly found along the
390 outer boundary of the study region with generally lower median elevations. The near absence of surging glaciers
391 in the inner Pamir with its generally higher median elevations is noteworthy. However, in the Mustagh region,
392 glaciers with observed surges have the highest (5646 m) and surging glaciers in the ‘Petr Alervogo west’ region
393 the lowest values (3429 m).

394

395 *Figure 10*

396

397 As surging glaciers have a bias towards larger sizes compared to all other glaciers (see Fig. 7), they also have
398 slightly higher elevation ranges (Fig. 11a) and form the upper end of the sample. However, the spread of values
399 for glaciers with a size of about 50 km² is very large, ranging from about 2000 to nearly 5000 m. The area-
400 elevation distribution in Fig. 11b displays a smaller amount of area around the mean elevation compared to all
401 other glaciers, which is likely due to the many small glaciers in these altitudes (see black circles in Fig. 10).

402

403 *Figure 11*

405 5.2 Observed changes

406 For a sample of 169 and 160 glaciers, we could map their minimum and maximum extent, respectively, and for
407 148 surges we determined the surge duration which is completely within the observation period. For 15 glaciers,
408 we observed a full surge cycle with the onset of the next surge and for six glaciers (Bivachny 63, Dzerzhinsky
409 104, Medvezhy 29, Right Dustiroz 31, Yazgulemdara 35, ObjectID 1) two or more surges were observed over the
410 study period. Both, the timing of the surges and their durations are highly variable (Fig. 12). Moreover, one has
411 to consider that several glaciers (>30) were already surging on the first available Landsat TM images (in 1988)
412 and several (>20) are still surging in 2017/2018. For both cases the surge duration could not be fully determined
413 and is thus longer than the values presented here.

414

415 *Figure 12*

416

417 The two histograms in Fig. 13 display a counting of the surges that started in a particular period (Fig. 13a) and of
418 the surge durations in 4-year bins (Fig. 13b). For Fig. 13a it has to be considered that the first period (1988/89) is
419 including only glaciers that started surging in 1989 because it is unclear in which year the glaciers with a 1988
420 starting year actually started surging. For the surge duration counting in Fig. 13b this means that shorter surge
421 periods are over-represented and are indeed longer. Furthermore, the last period is not complete (i.e. surges are
422 on-going), which has the same effect on the counting. This results in likely too high and too low values in the
423 first and last period, respectively. To circumvent this bias, we have also counted all surges that took fully place
424 within the period, i.e. started after 1989 and ended before 2017 (grey bars in Fig. 13b). This sample is now
425 smaller, but has still a reasonable number of glaciers in all classes. Figure 13a reveals that the number of surges
426 that have started in the second and third period is the same and slowly declining afterwards. The surge duration
427 counting displayed in Fig. 13b has a peak at 1-5 years and very similar numbers for the next four intervals. Only
428 few glaciers (9) have surge durations exceeding 21 years. The combination start year and duration gives the
429 number of glaciers that are surging in a particular year. We found a steady increase in this number from 1990
430 (54) to 2000 (114), with a plateau until 2008 (112) and a steady decrease afterwards (to 72 in 2018). In other
431 words, in any year during the observation period at least 54 glaciers were actively surging in the study region, up
432 to a maximum of 129 glaciers in 2006. This is far more than we expected.

433

434 *Figure 13*

435

436 The simplified typology (see Section 4.2) counting presented in Table 4 reveals that 75% of all glaciers have
437 freely advancing tongues, whereas 18% only connect to another glacier at least in their maximum extent. The rest
438 are tributaries. From the total sample of identified surging glaciers, 85% (169 glaciers) are considerably
439 advancing whereas the remaining 15% (26 glaciers) are surging internally with none or only a minor terminus
440 advance. The latter were sometimes hard to detect and required application of additional measures (see Section
441 3). From the glaciers with a substantial terminus advance, most (62%) advance up to 1 km. Larger advances of up

442 to 2.5 km are found for 31% of the glaciers and 7.6% advanced more than 2.5 km (up to 6.7 km). Most of the
443 surges with a change in terminus position are situated in the central mountain ranges around Fedchenko Glacier,
444 whereas the eastern ranges are dominated by stable glaciers and internal surges (but with a high variability). The
445 strongest advance has been Oshanina Glacier (9) in the Petr Alervogo East mountain range with 4078 m. For this
446 analysis, we excluded all glacier surges that were not fully covered by the observation period (start before 1988,
447 end after 2018).

448

449 *Table 4*

450

451 One of the most active glaciers is Medvezhy Glacier (29) with a surge cycle of only ~10 years and an active
452 period of just 2 years (Kotlyakov et al., 2018). Further glaciers with relatively short (≤ 5 years) active phases are
453 spread all over the study region. During the active surge phase, 128 glaciers increased their area by a total of
454 ~119 km², which is 6% of their total area (GI-3min) and 4% of the total area in the GI-2 inventory. On average,
455 the minimum elevation decreased from 3954 m a.s.l. to 3793 m a.s.l., but individual glaciers are reaching to more
456 than 800 m lower elevations at their maximum extent. The change in minimum elevation due to a surge does not
457 depend on the elevation range (or size) of the glacier. This is also related to the fact that several large glaciers
458 show mostly internal surges with maybe only a small advance of the tongue. Similarly, also length changes due
459 to a surge do not depend on glacier size or length. However, it is noteworthy that some glaciers change their
460 length by about a factor of almost two (ObjectID 41).

461 **6. Discussion**

462 **6.1 Characteristics of the surging glaciers and their surges**

463 Surging glaciers dominate the area classes above 10 km², which would confirm earlier observations that surging
464 glaciers are comparably large (Barrand and Murray, 2006; Clarke et al., 1986; Mukherjee et al., 2017). However,
465 we found that they can also be smaller than 1 km², down to 0.3 km². Why such small glaciers surge, often
466 increasing their length considerably, needs to be further investigated. We also have to mention that there might be
467 even smaller glaciers that were not detected due to the coarse resolution of the satellite data, i.e. our sample is
468 somewhat biased towards larger glaciers. Whereas the aspect distribution of surging glaciers is very similar to all
469 other glaciers (Fig. 8), they seem to have lower median elevations than other glaciers when facing north and
470 higher ones when facing south (Fig. 9). We do not have a physical explanation for this and assume it might only
471 be an artefact of the sampling. Their spatial distribution, on the other hand, is more peculiar as they are mostly
472 found in the outer regions of the study site (Figs. 5 and 10). Their higher share of large elevation ranges (Fig.
473 11a) is related to their generally larger size and their hypsometry is very similar to other glaciers.

474

475 Within the period considered here, the starting dates of surges are comparably random (Fig. 12), indicating a
476 limited impact of climatic trends on the timing. The high number of surging glaciers (about 55 to max 120) in any
477 year is remarkable and can only be found in the Karakoram (Bhambri et al., 2017). Whether the constant increase
478 before the year 2000 and decline after 2008 is an artefact of the sampling or has other reasons needs to be

479 investigated in a further study. A comparable increase in glacier surge activity after 1990 was also found in the
480 Karakoram by (Copland et al., 2011). Surge durations (11 years in the mean) are as diverse as in the Karakoram
481 (Bhambri et al., 2017; Paul, 2020). However, complete surge cycles (from the start of an active phase to the next)
482 are only observed for a few glaciers, so this impression is biased by the observation window. Due to gaps in
483 satellite data availability, we might have missed a few glaciers displaying only (short) internal surges, so the real
484 number of surging glaciers might be even higher and the number of glaciers with a short duration of active phases
485 higher than in our sample.

486 **6.2 Criteria to identify surges**

487 The criteria we applied to identify surges were handled flexibly to consider the wide range of surge types found
488 in the region. However, the differentiation between surging and ‘only’ advancing glaciers is sometimes
489 challenging and other interpretations are possible. The very high-resolution images as available for our study site
490 from Corona / Hexagon and Google Earth / Bing Maps did not help much in determining the timing of a surge
491 (due to the large temporal gaps), but were most helpful in confirming the surge nature of a glacier in previous and
492 recent times, respectively (Lv et al. 2019, Paul 2020). The historic images clearly reveal that many glaciers in the
493 Pamir Mountains have also surged in the 1970s, however we have not used them here to derive the timing of
494 these earlier surges as this would be a large additional exercise and the temporal density of available images
495 might not be sufficient. However, we used them to confirm additional minimum and maximum extents.

496 **6.3 Uncertainties**

497 Regarding the uncertainties of the derived topographic characteristics, one has to consider that we used the GI-1
498 basis inventory from around 2000 with a DEM (GDEMv3) from around 2008 (NASA, 2018). The DEM has local
499 artefacts, is void filled and the timing of both datasets does not match. The latter is in particular the case for
500 glaciers that surged between 2000 and 2009 and had strong changes in geometry. The strongest impact is likely
501 on minimum elevation, but also median elevation, aspect and mean slope might be impacted. There is little we
502 can do about this uncertainty, as otherwise we would need a DEM from nearly every year, synchronous with the
503 timing of the minimum glacier extent. However, for the overall statistical analysis of the datasets presented here,
504 the impact of the temporal mismatch on the graphs is likely small. Of course, when individual glaciers are
505 analysed, this mismatch has to be considered (Frey and Paul, 2012).

506
507 Regarding the timing of the observed surges, we face the following uncertainties:

508 a) We have only analysed the time window 1988 to 2018; the assigned duration of surges starting before 1988 or
509 ending after 2018 is thus too short,

510 b) we only include glaciers with an active surge phase between 1988 and 2018; the real number of glaciers in the
511 study region that surged in the past might thus be higher,

512 c) for most regions we do not have usable satellite images in every year (e.g. due to snow and clouds); this adds
513 to the uncertainty of the start/end assignment and could even result in completely missed short-lived internal
514 surges,

515 d) the spatial resolution of Landsat sometimes impacts a proper identification of the terminus, in particular when
516 debris-covered; this leads to uncertainties in the timing,
517 e) due to residual dead ice in the glacier forefield and debris cover, the timing of the minimum extent is more
518 difficult to define than the maximum; in uncertain cases we used the extent from GI-3, and
519 f) when surges start with a mass wave and/or stay internal (no terminus advance), the timing derived from visual
520 analysis will likely be different from studies analysing flow velocities.
521 Collectively, it is likely that other analysts derive different start/end dates of individual surges, but in most cases
522 the difference will not exceed a few years. This will thus not affect the overall conclusions about the highly
523 variable timing of surges and surge durations.

524

525 The assignment of surge classes presented here should be robust as we used qualitative and categorised criteria
526 that will not change much for a different interpretation. However, not all surges of the same glacier end up in the
527 same class. For example, if a recent surge is more dynamic than a previous one, it might reach another glacier
528 and become a part-time tributary. Also internal surges might have shown advancing termini before and are thus
529 not strictly internal. Hence, the assigned classes can vary for other surges. In general, we only assigned the
530 characteristics of the surge of the main glacier trunk to the attribute table.

531 **6.4 Comparison to other inventories**

532 Compared to previous studies, we identified several new surging glaciers. Some of the probable or possible
533 (category 2 and 3) surges listed in Osipova et al. (1998) have indeed surged and are now included in our
534 inventory. Most others found in these categories could not be confirmed as the morphological details used to
535 identify surge activities are only visible in very high-resolution imagery (at least 2 m) rather than with 30 or 15 m
536 Landsat data we used here. It is, however, well possible that they surged outside our observation window.

537

538 Sevestre and Benn (2015) presented 820 possible surge-type glaciers in the Pamir mainly based on the inventory
539 by Osipova et al. (1998). Our findings are in good agreement with the 51 most reliably classified (category 3)
540 surge-type glaciers marked in the RGI (we include 45 of them). Our 132 additional surging glaciers belong
541 mostly (55 of 188) to category (2 – probably surging) in the RGI, and a few (18 of 322) belong to category (1 –
542 possibly surging). The remaining 52 surging glaciers were not indicated as surge-type in the RGI. When
543 considering the 14 further glaciers which were mentioned by Lv et al. (2019), 38 (20.5% of the total sample) so
544 far unknown surging glaciers have been identified here for the Pamir. Outlines from two of our surging glaciers
545 (ObjectIDs 65 and 64) are missing in the RGI 6.0.

546

547 Compared to Lv et al. (2019), we identified three further surging glaciers (16 in total) in the King Tau and
548 Ulugarttag sub-regions. Apart from surge-type glaciers, their study also classified four glaciers as advancing,
549 eleven as stable and one retreating. We classified one of their advancing and three of their stable glaciers as
550 surging. This new interpretation results from our longer observation period and the DEM difference images
551 revealing the typical mass redistribution patterns. The surging glaciers described by Kotlyakov et al. (2008) are in
552 full agreement with our findings. The above-mentioned numbers have to be interpreted with some care, as we

553 compared two different inventories with individual glacier divides. Thus, a direct and one-to-one comparison is
554 challenging.

555 **7. Conclusions**

556 In this study, we presented a new inventory of surging glaciers for the Pamir Mountains. The analysis is based on
557 results from earlier studies, Landsat imagery acquired over the period 1988 to 2018, the SRTM, ASTER
558 GDEMv3 and ALOS DEM, and declassified very-high resolution images from Corona and Hexagon as well as
559 more recent very high-resolution satellite data (Bing Maps & Google Earth). Using animations and flicker images
560 for the Landsat time series in combination with the elevation change patterns from DEM differencing, we
561 detected 206 spatially distinct glacier surges within 186 glacier bodies. The new dataset is in good agreement
562 with previous compilations of surging glaciers and confirmed surges for 133 new glaciers that were so far only
563 marked as surge-type probable or possible. We further digitized minimum and maximum extent of 169 and 160
564 glaciers, respectively, and determined the timing for about $\frac{3}{4}$ of all surges. The temporal distribution is random
565 concerning timing and surge duration (mean value 11 years), but the high number of active surges in any year
566 (between 54 and 120) was unexpected and has only previously been observed in the Karakoram. The distribution
567 of surging glaciers is biased towards the central, northern and eastern mountain ranges. Their sizes range from
568 0.3 to 143 km² and they are dominating the size-class distribution above 10 km². Three glaciers descend by more
569 than 800 m and five increased their length by a factor of more than 2 during a surge. However, advance distances
570 are not related to original glacier length as several large glaciers only show internal surges or very small
571 advances. The three inventories created in this study (GI-3, GI-3min, GI-3max) are available in the Supplemental
572 Material to serve as a base for further investigations.

573 **8. Data availability**

574 The dataset can be downloaded from: <https://doi.pangaea.de/10.1594/PANGAEA.914150> (Goerlich et al., 2020).

575 **Author contribution**

576 F.G. and F.P. designed the study, analysed the datasets and wrote the manuscript, F.G. processed the data and
577 prepared all figures and datasets. T.B. provided additional literature and datasets. All authors contributed to the
578 writing and editing of the manuscript.

579 **Competing interests**

580 The authors declare that they have no conflict of interest.

581 **Acknowledgements**

582 The work of F.G. and F.P. was supported by the ESA projects Glaciers_cci (4000109873/14/I-NB) and
583 Glaciers_cci+ (4000127593/19/I-NB), the work of T.B. was partially supported by the Strategic Priority Research
584 Program of Chinese Academy of Sciences (XDA20100300). The AW3D30 DEM is provided by the Japan
585 Aerospace Exploration Agency (<http://www.eorc.jaxa.jp/ALOS/en/aw3d30/index.htm>) ©JAXA. All Corona,
586 Hexagon and Landsat images used in this study were provided by USGS and downloaded from
587 earthexplorer.usgs.gov. We thank P. Rastner for supporting us in calculating the topographic parameters for
588 several states of the inventory, K. Mukherjee for providing the Hexagon DEMs from 1975 and H. Machguth for
589 providing the centre lines for determination of glacier length and length changes. We thank the two anonymous
590 reviewers for their conscientious work to improve this study.

- 592 Barrand, N. E. and Murray, T.: Multivariate Controls on the Incidence of Glacier Surging in the Karakoram
593 Himalaya, Arctic, Antarct. Alp. Res., 38(4), 489–498, doi:10.1657/1523-
594 0430(2006)38[489:MCOTIO]2.0.CO;2, 2006.
- 595 Berthier, E. and Brun, F.: Karakoram geodetic glacier mass balances between 2008 and 2016: Persistence of the
596 anomaly and influence of a large rock avalanche on Siachen Glacier, *J. Glaciol.*, 65(251), 494–507,
597 doi:10.1017/jog.2019.32, 2019.
- 598 Bhambri, R., Hewitt, K., Kawishwar, P. and Pratap, B.: Surge-type and surge-modified glaciers in the
599 Karakoram, *Sci. Rep.*, 7(15391), 1–14, doi:10.1038/s41598-017-15473-8, 2017.
- 600 Bolch, T., Pieczonka, T., Mukherjee, K. and Shea, J.: Brief communication: Glaciers in the Hunza catchment
601 (Karakoram) have been nearly in balance since the 1970s, *Cryosphere*, 11(1), 531–539, doi:10.5194/tc-11-
602 531-2017, 2017.
- 603 Brun, F., Berthier, E., Wagnon, P., Kääb, A. and Treichler, D.: A spatially resolved estimate of High Mountain
604 Asia glacier mass balances from 2000 to 2016, *Nat. Geosci.*, 10(9), 668–673, doi:10.1038/ngeo2999, 2017.
- 605 Clarke, K. C., Sciamoi, P., Simon, C. and Ommanney, L.: Characteristics of Surge-Type Glaciers, *J. Geophys.*
606 *Res.*, 91(5), 7165–7180, doi:10.1029/JB091iB07p07165, 1986.
- 607 Copland, L., Sylvestre, T., Bishop, M. P., Shroder, J. F., Seong, Y. B., Owen, L. A., Bush, A. and Kamp, U.:
608 Expanded and Recently Increased Glacier Surging in the Karakoram, Arctic, Antarct. Alp. Res., 43(4), 503–
609 516, doi:10.1657/1938-4246-43.4.503, 2011.
- 610 Dolgushin, L. D. and Osipova, G. B.: New Data on the recent Glacier Surges, *Mater. Glyatsiol.*, 18, 191–217,
611 1971.
- 612 Dolgushin, L. D. and Osipova, G. B.: Glacier surges and the problem of their forecasting, *IAHS Publ.* (104),
613 292–304, 1975.
- 614 Dowdeswell, J. A., Gorman, M. R., Macheret, Y. Y., Moskalevsky, M. Y. and Hagen, J. O.: Digital comparison
615 of high resolution Sojuzkarta KFA-1000 imagery of ice masses with Landsat and SPOT data, *Ann. Glaciol.*,
616 17, 105–112, doi:10.3189/S0260305500012684, 1993.
- 617 Dowdeswell, J. A., Glazovsky, A. F. and Macheret, Y. Y.: Ice divides and drainage basins on the ice caps of
618 Franz Josef Land, Russian High Arctic, defined from Landsat, KFA-1000, and ERS-1 SAR satellite imagery,
619 *Artic Alp. Res.*, 27(3), 264–270, doi:10.1080/00040851.1995.12003121, 1995.
- 620 Falaschi, D., Bolch, T., Lenzano, M. G., Tadono, T., Lo Vecchio, A. and Lenzano, L.: New evidence of glacier
621 surges in the Central Andes of Argentina and Chile, *Prog. Phys. Geogr.*, 42(6), 792–825,
622 doi:10.1177/0309133318803014, 2018.
- 623 Finaev, A. F., Shiyin, L., Weijia, B. and Li, J.: Climate Change And Water Potential Of The Pamir Mountains,
624 *Geogr. Environ. Sustain.*, 9(3), 88–105, doi:10.15356/2071-9388_03v09_2016_06, 2016.
- 625 Frey, H. and Paul, F.: On the suitability of the SRTM DEM and ASTER GDEM for the compilation of:
626 Topographic parameters in glacier inventories, *Int. J. Appl. Earth Obs. Geoinf.*, 18(1), 480–490,
627 doi:10.1016/j.jag.2011.09.020, 2012.
- 628 Galiatsatos, N.: The Shift from Film to Digital Product: Focus on CORONA Imagery, *Photogramm. -*
629 *Fernerkundung - Geoinf.*, 2009(3), 251–260, doi:10.1127/0935-1221/2009/0020, 2009.
- 630 Gardelle, J., Berthier, E., Arnaud, Y. and Kääb, A.: Region-wide glacier mass balances over the Pamir-
631 Karakoram-Himalaya during 1999-2011, *Cryosphere*, 7(4), 1263–1286, doi:10.5194/tc-7-1263-2013, 2013.
- 632 Goerlich, F., Bolch, T., Mukherjee, K. and Pieczonka, T.: Glacier Mass Loss during the 1960s and 1970s in the
633 Ak-Shirak Range (Kyrgyzstan) from Multiple Stereoscopic Corona and Hexagon Imagery, *Remote Sens.*,
634 9(275), doi:10.3390/rs9030275, 2017.
- 635 Goerlich, F., Bolch, T., Paul, F.: Inventory of surging glaciers in the Pamir. PANGAEA,
636 <https://doi.pangaea.de/10.1594/PANGAEA.914150>, 2020.
- 637 Herreid, S. and Truffer, M.: *Journal of Geophysical Research : Earth Surface* Automated detection of unstable
638 glacier flow and a spectrum of speedup behavior in the Alaska Range Special Section :, *J. Geophys. Res.*
639 *Earth Surf.*, 121(1), 64–81, doi:10.1002/2015JF003502.Surge-type, 2016.
- 640 Holzer, N., Golletz, T., Buchroithner, M. F. and Bolch, T.: Glacier Variations in the Trans Alai Massif and the
641 Lake Karakul Catchment (Northeastern Pamir) Measured from Space, in R.P. Singh, U. Schikhoff, & S. Mal
642 (Eds.): *Climate Change, Glacier Response, and Vegetation Dynamics in the Himalaya*, edited by R. P. Singh,
643 U. Schikhoff, and S. Mal, pp. 139–153, Springer, Cham., 2016.
- 644 Kääb, A., Isakowski, Y., Paul, F., Neumann, A. and Winter, R.: Glaziale und periglaziale Prozesse: Von der
645 statischen zur dynamischen Visualisierung, *Kartographische Nachrichten*, 53(5), 206–212, 2003.
- 646 Kotlyakov, V. M., Desinov, L. V., Osipova, G. B., Hauser, M., Tsvetkov, D. G. and Schneider, J. F.: Events in
647 2002 on Russian Geographical Society (RGO) Glacier, Pamirs, *Mater. Glyatsiol.*, 95, 221–230, 2003.

- 648 Kotlyakov, V. M., Osipova, G. B. and Tsvetkov, D. G.: Monitoring of the Pamirs surging glaciers from space,
649 *Ann. Glaciol.*, 48, 125–134, doi:10.3189/172756408784700608, 2008.
- 650 Kotlyakov, V. M., Chernova, L. P., Khromova, T. E., Muraviev, A. Y., Kachalin, A. B. and Tiufin, A. S.:
651 Unique Surges of Medvezhy Glacier, *Dokl. Earth Sci.*, 483(2), 1547–1552, doi:10.1134/s1028334x18120152,
652 2018.
- 653 Lambrecht, A., Mayer, C., Aizen, V., Floricioiu, D. and Surazakov, A.: The evolution of Fedchenko glacier in the
654 Pamir, Tajikistan, during the past eight decades, *J. Glaciol.*, 60(220), 233–244, doi:10.3189/2014JoG13J110,
655 2014.
- 656 Lambrecht, A., Mayer, C., Wendt, A., Floricioiu, D. and Völksen, C.: Elevation change of Fedchenko Glacier,
657 Pamir Mountains, from GNSS field measurements and TanDEM-X elevation models, with a focus on the
658 upper glacier, *J. Glaciol.*, 64(246), 637–648, doi:10.1017/jog.2018.52, 2018.
- 659 Liang, L., Cuo, L. and Liu, Q.: The energy and mass balance of a continental glacier: Dongkemadi Glacier in
660 central Tibetan Plateau, *Sci. Rep.*, 8(1), 1–8, doi:10.1038/s41598-018-31228-5, 2018.
- 661 Lv, M., Guo, H., Lu, X., Liu, G., Yan, S., Ruan, Z., Ding, Y. and Quincey, D. J.: Characterizing the behaviour of
662 surge- and non-surge-type glaciers in the Kingata Mountains, eastern Pamir, from 1999 to 2016, *Cryosphere*,
663 13(1), 219–236, doi:10.5194/tc-13-219-2019, 2019.
- 664 Machguth, H. and Huss, M.: The length of the world’s glaciers a new approach for the global calculation of
665 center lines, *Cryosphere*, 8(5), 1741–1755, doi:10.5194/tc-8-1741-2014, 2014.
- 666 Maussion, F., Scherer, D., Mölg, T., Collier, E., Curio, J. and Finkelnburg, R.: Precipitation seasonality and
667 variability over the Tibetan Plateau as resolved by the high Asia reanalysis, *J. Clim.*, 27(5), 1910–1927,
668 doi:10.1175/JCLI-D-13-00282.1, 2014.
- 669 Meier, M. F. and Post, A.: What are glacier surges?, *Can. J. Earth Sci.*, 6(4(2)), 807–817, 1969.
- 670 Minora, U., Bocchiola, D., D’Agata, C., Maragno, D., Mayer, C., Lambrecht, A., Vuillermoz, E., Senese, A.,
671 Compostella, C., Smiraglia, C. and Diolaiuti, G. A.: Glacier area stability in the Central Karakoram National
672 Park (Pakistan) in 2001–2010: The “Karakoram Anomaly” in the spotlight., 2016.
- 673 Mölg, N., Bolch, T., Rastner, P., Strozzi, T. and Paul, F.: A consistent glacier inventory for Karakoram and Pamir
674 derived from Landsat data: Distribution of debris cover and mapping challenges, *Earth Syst. Sci. Data*, 10(4),
675 1807–1827, doi:10.5194/essd-10-1807-2018, 2018.
- 676 Mukherjee, K., Bolch, T., Goerlich, F., Kutuzov, S., Osmonov, A., Pieczonka, T. and Shesterova, I.: Surge-type
677 glaciers in the Tien Shan (Central Asia), Arctic, *Antarct. Alp. Res.*, 49(1), 147–171,
678 doi:10.1657/AAAR0016-021, 2017.
- 679 NASA/METI/AIST/Japan Spacesystems and U.S./Japan ASTER Science Team: ASTER Global Digital
680 Elevation Model V003 [Data Set]., 2018.
- 681 Osipova, G. B., Tsvetkov, D. G., Schetinnikov, A. S. and Rudak, M. S.: Inventory of surging glaciers of the
682 Pamirs, *Mater. Glyatsiol.*, 85, 3–136, 1998.
- 683 Osipova, G. B. and Khromova, T. E.: Electronic data base “Surging glaciers of Pamir” *Ice Snow*, 50(4), 15–24,
684 2010. (in Russian)
- 685 Osipova, G. B.: Fifty years of studying the Medvezhiy Glacier (West Pamirs) by the Institute of Geography,
686 RAS, *Ice Snow*, 1, 129–140, doi:10.15356/2076-6734-2015-1-129-140, 2015.
- 687 Paul, F.: Revealing glacier flow and surge dynamics from animated satellite image sequences: Examples from the
688 Karakoram, *Cryosphere*, 9(6), 2201–2214, doi:10.5194/tc-9-2201-2015, 2015.
- 689 Paul, F.: A 60-year chronology of glacier surges in the central Karakoram from the analysis of satellite image
690 time-series, *Geomorphology*, 352, 106993, doi:10.1016/j.geomorph.2019.106993, 2020.
- 691 Paul, F., Kääb, A., Maisch, M., Kellenberger, T. and Haerberli, W.: The new remote-sensing-derived Swiss
692 glacier inventory: I. Methods, *Ann. Glaciol.*, 34, 355–361, doi:10.3189/172756402781817473, 2002.
- 693 Paul, F., Barry, R. G., Cogley, J. G., Frey, H., Haerberli, W., Ohmura, A., Ommanney, C. S. L., Raup, B., Rivera,
694 A. and Zemp, M.: Recommendations for the compilation of glacier inventory data from digital sources, *Ann.*
695 *Glaciol.*, 50(53), 119–126, doi:10.3189/172756410790595778, 2009.
- 696 Pieczonka, T., Bolch, T. and Buchroithner, M.: Generation and evaluation of multitemporal digital terrain models
697 of the Mt. Everest area from different optical sensors, *ISPRS J. Photogramm. Remote Sens.*, 66(6), 927–940,
698 doi:10.1016/j.isprsjprs.2011.07.003, 2011.
- 699 Pieczonka, T., Bolch, T., Junfeng, W. and Shiyin, L.: Heterogeneous mass loss of glaciers in the Aksu-Tarim
700 Catchment (Central Tien Shan) revealed by 1976 KH-9 Hexagon and 2009 SPOT-5 stereo imagery, *Remote*
701 *Sens. Environ.*, 130, 233–244, doi:10.1016/j.rse.2012.11.020, 2013.
- 702 Quincey, D. J., Glasser, N. F., Cook, S. J. and Luckman, A.: Heterogeneity in Karakoram glacier surges, *J.*
703 *Geophys. Res. Earth Surf.*, 120(7), 1288–1300, doi:10.1002/2015JF003515, 2015.
- 704 Rabus, B., Eineder, M., Roth, A. and Bamler, R.: The shuttle radar topography mission—a new class of digital
705 elevation models acquired by spaceborne radar, *ISPRS J. Photogramm. Remote Sens.*, 57(4), 241–262,
706 doi:10.1016/S0924-2716(02)00124-7, 2003.

- 707 Rankl, M. and Braun, M.: Glacier elevation and mass changes over the central Karakoram region estimated from
708 TanDEM-X and SRTM/X-SAR digital elevation models, *Ann. Glaciol.*, 57(71), 273–281,
709 doi:10.3189/2016AoG71A024, 2016.
- 710 Round, V., Leinss, S., Huss, M., Haemmig, C. and Hajnsek, I.: Surge dynamics and lake outbursts of Kyagar
711 Glacier, Karakoram, *Cryosphere*, 11(2), 723–739, doi:10.5194/tc-11-723-2017, 2017.
- 712 Sevestre, H. and Benn, D. I.: Climatic and geometric controls on the global distribution of surge-type glaciers:
713 Implications for a unifying model of surging, *J. Glaciol.*, 61(228), 646–662, doi:10.3189/2015JoG14J136,
714 2015.
- 715 Shean, D.: High Mountain Asia 8-meter DEM Mosaics Derived from Optical Imagery, Version, Boulder,
716 Colorado., 2017.
- 717 Steiner, J. F., Kraaijenbrink, P. D. A., Jiduc, S. G. and Immerzeel, W. W.: Brief Communication : The Khurdopin
718 glacier surge revisited – extreme flow velocities and formation of a dammed lake in 2017, *Cryosph.*, 12(1),
719 95–101, 2018.
- 720 Takaku, J., Tadono, T. and Tsutsui, K.: Generation of high resolution global DSM from ALOS PRISM, *Int. Arch.*
721 *Photogramm. Remote Sens. Spat. Inf. Sci. - ISPRS Arch.*, 40(4), 243–248, doi:10.5194/isprsarchives-XL-4-
722 243-2014, 2014.
- 723 Wendt, A., Mayer, C., Lambrecht, A. and Floricioiu, D.: A Glacier Surge of Bivachny Glacier, Pamir Mountains,
724 Observed by a Time Series of High-Resolution Digital Elevation Models and Glacier Velocities, *Remote*
725 *Sens.*, 9(4), 388, doi:10.3390/rs9040388, 2017.
- 726 Wessel, B.: TanDEM-X Ground Segment – DEM Products Specification Document”, Oberpfaffenhofen. [online]
727 Available from: <https://tandemx-science.dlr.de/>, 2016.
- 728 Yasuda, T. and Furuya, M.: Dynamics of surge-type glaciers in West Kunlun Shan, Northwestern Tibet, *J.*
729 *Geophys. Res. F Earth Surf.*, 120(11), 2393–2405, doi:10.1002/2015JF003511, 2015.
- 730 Zhang, H., Zhang, F., Zhang, G., Ma, Y., Yang, K. and Ye, M.: Daily air temperature estimation on glacier
731 surfaces in the Tibetan Plateau using MODIS LST data, *J. Glaciol.*, 64(243), 132–147,
732 doi:10.1017/jog.2018.6, 2018.
- 733

734 Tables

735

736 *Table 1: Main characteristics of the satellite scenes used (see Table S1 for scene list).*

Satellite	Sensor	Resolution	Period	Purpose
Corona	KH-4	2-5 m	1968	DEM generation, high-res. info
Hexagon	KH-9	5-10 m	1975/1980	Additional DEM and high-res. info
Landsat	MSS	60 m	1972-1980	Extension back in time
Landsat	TM	30 m	1989-2012	Animation
Landsat	ETM+	30 m	1999-2018	Animation
Landsat	OLI	30 m	2013-2018	Animation

737

738

739 *Table 2: Selected characteristics of available DEMs and their usage in this study.*

DEM	Type	Sensor	Resolu tion	Acquisition period	Date of tiles?	Usage
GDEMv3	optical	ASTER	30 m	2000-2013	No	Heights for Corona, topographic parameters
SRTM	SAR-C	SRTM	30 m	Feb 2000	Yes	Elevation changes
ALOS	optical	PRISM	30 m	2007-2011	No	elevation changes 2000 to 2009
TDX	SAR-X	TanDEM-X	90 m	2012-2015	No	Elevation changes ~2009 to ~2014
Corona	optical	KH4-B	15 m	1968	Yes	Elevation changes 1968 to 2000; Orthophoto

740

741 *Table 3: Size class distribution of surging glaciers and other glaciers of GI-2 and GI-3.*

Size Class km ²	<0.05	0.05	0.1	0.5	1	5	10	50	100	>500	
		–	–	–	–	–	–	–	–	–	
		0.1	0.5	1	5	10	50	100	500		
other	km ²	103.7	154.7	1104	1090.7	3353.4	1172.7	1190.1	167.8	154	580.3

glaciers	%	1.1	1.7	12.2	12	37	12.9	13.1	1.9	1.7	6.4
surging	km ²	0	0	0.4	6.1	174.2	319.7	1229	682.9	262.6	0
glaciers	%	0	0	0	0.2	6.5	12	46	25.5	9.8	0
all	km ²	103.7	154.7	1104.5	1096.9	3527.6	1492.3	2419.2	850.6	416.6	580.3
glaciers	%	0.9	1.3	9.4	9.3	30	12.7	20.6	7.2	3.5	4.9
Surging proportion in %		0	0	0	0	0	21.4	50.8	80.3	63	0

742

743

744 *Table 4: Results of the surging classification (counting per class). Glaciers with incomplete active surge phases*

745 *(starting before 1988 or ending after 2018 and marked with a “0” for the distance criterion) are not listed here.*

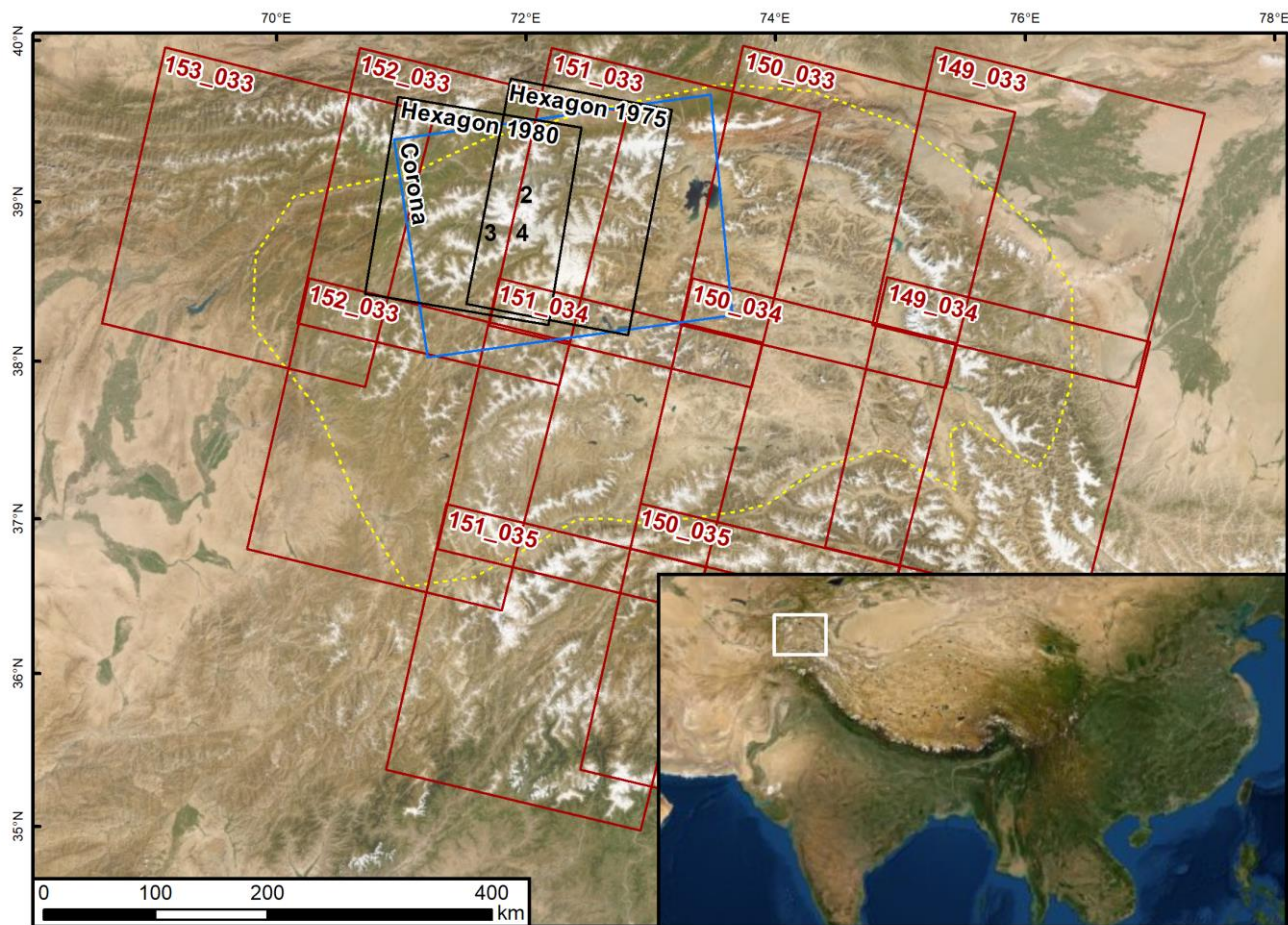
746 *See Section 4.2 for the meaning of classes 1, 2, and 3.*

Criteria	1	2	3	Total
Tongue	150	32	16	198
Type	169	25	4	198
Duration	21	63	114	198
Distance	106	53	13	172

747

748

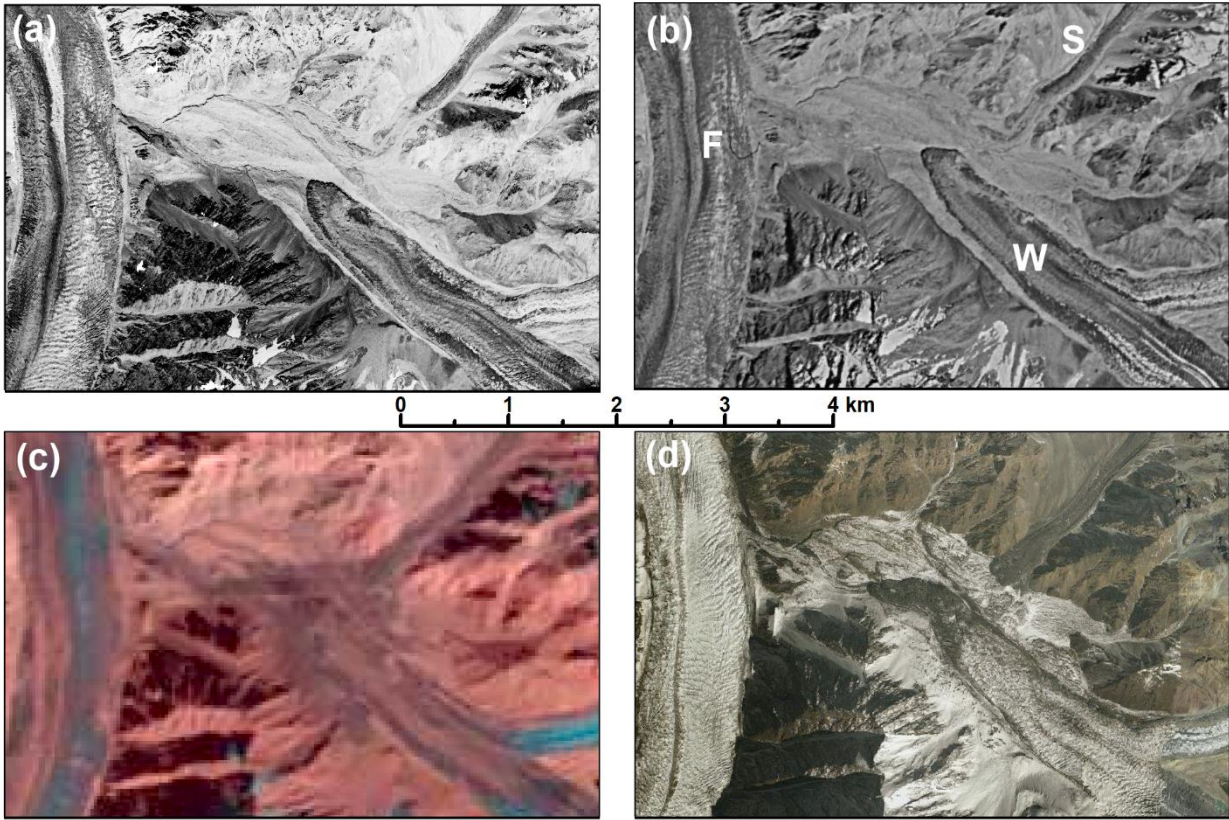
750



751

752 *Fig. 1: Location of the study region (white square in the inset) and footprints of the Corona (blue), Hexagon*
 753 *(black) and Landsat (red) scenes used in this study. The dashed yellow line marks the perimeter of the study*
 754 *region. The location of the sub-regions displayed in Figs. 2, 3 and 4 are marked with their respective numbers.*
 755 *Image sources: screenshots from © Google Earth.*

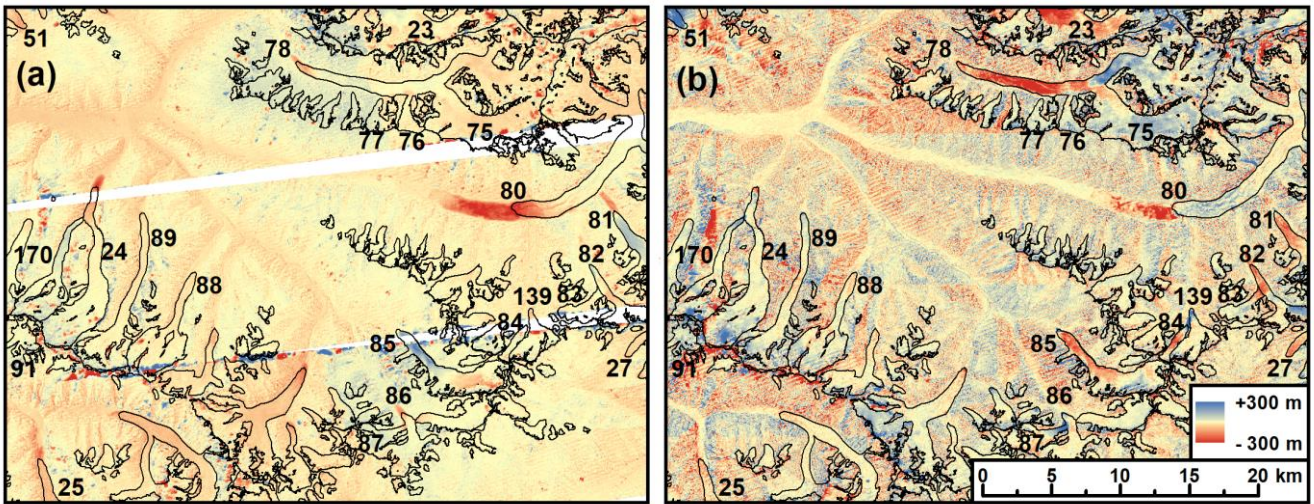
756



757

758 Fig. 2: Comparison of satellite images for the same sub-region (see Fig. 1 for location) showing the following
 759 glaciers: F: Fortambek (18), W: Walter 731 (19), and S: Soldatov (20). The images are acquired by a) Corona in
 760 1968, b) Hexagon in 1975, c) Landsat in 2017, and d) Bing Maps (date unknown). Image sources: Panels a) to c)
 761 earthexplorer.usgs.gov, panel d) screenshot from bing.com ©2020 DigitalGlobe.

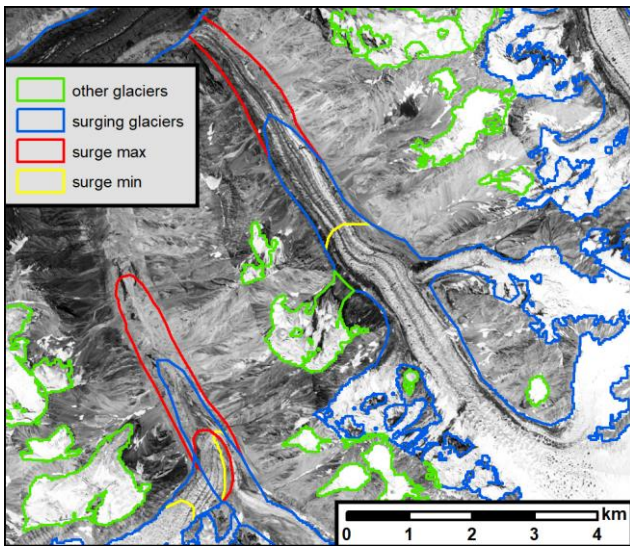
762



763

764 Fig. 3: Two examples of colour-coded DEM difference images used to identify surging glaciers (marked with
 765 their ObjectID). The glacier outlines depict the glacier state in ~2000 (GI-2). A) SRTM-Corona (2000-1968) and
 766 b) AW3D30-SRTM (~2010-2000).

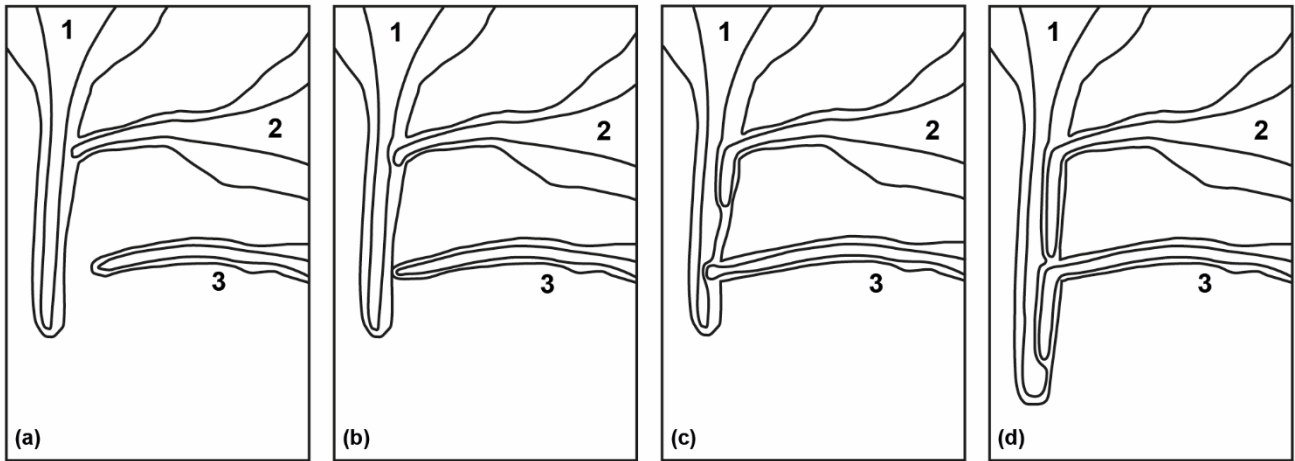
767



768

769 Fig. 4: Comparison of glacier outlines from the original inventory GI-2 (blue/green)
 770 / GI-3max (yellow/red) showing the minimum and maximum extents of two surging glaciers. Image acquisition
 771 date and source: 1968, earthexplorer.usgs.gov.

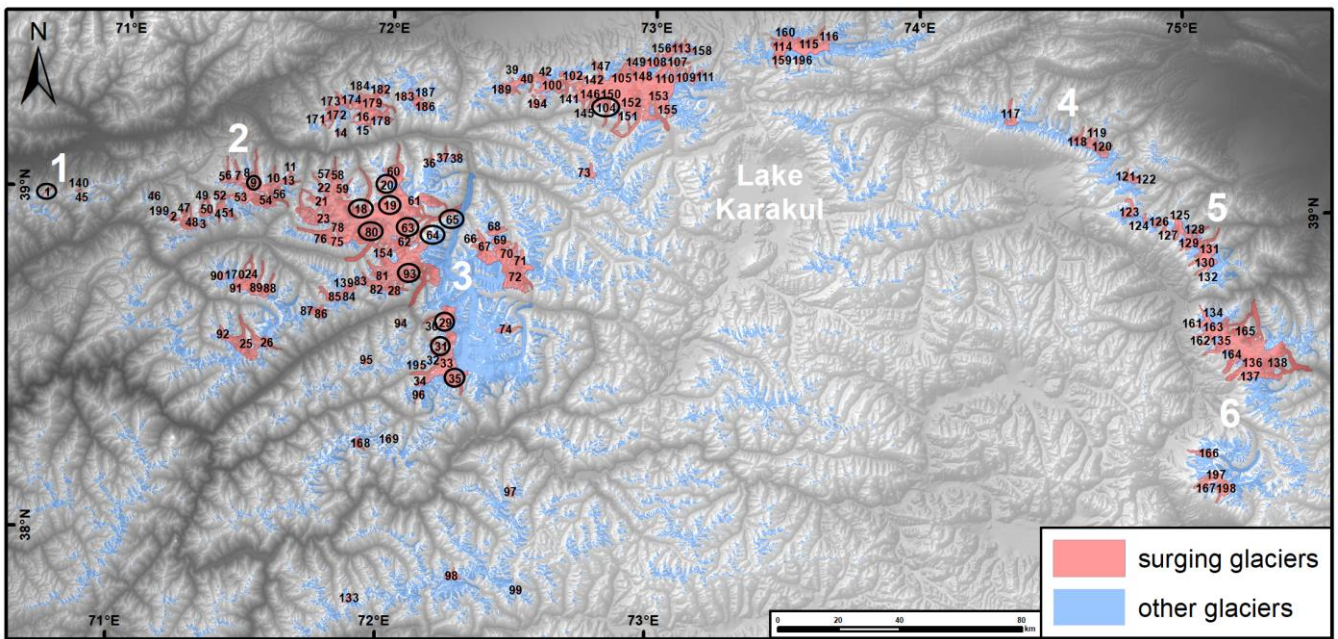
772



773

774 Fig. 5: Sketch map of selected possible interactions among surging glaciers of different types. a) At the beginning
 775 – glacier 2 in full surge mode, b) surge maximum of glacier 2 and surge start of glacier 3, c) surge maximum of
 776 glacier 3, d) surge of glacier 1. See text for description.

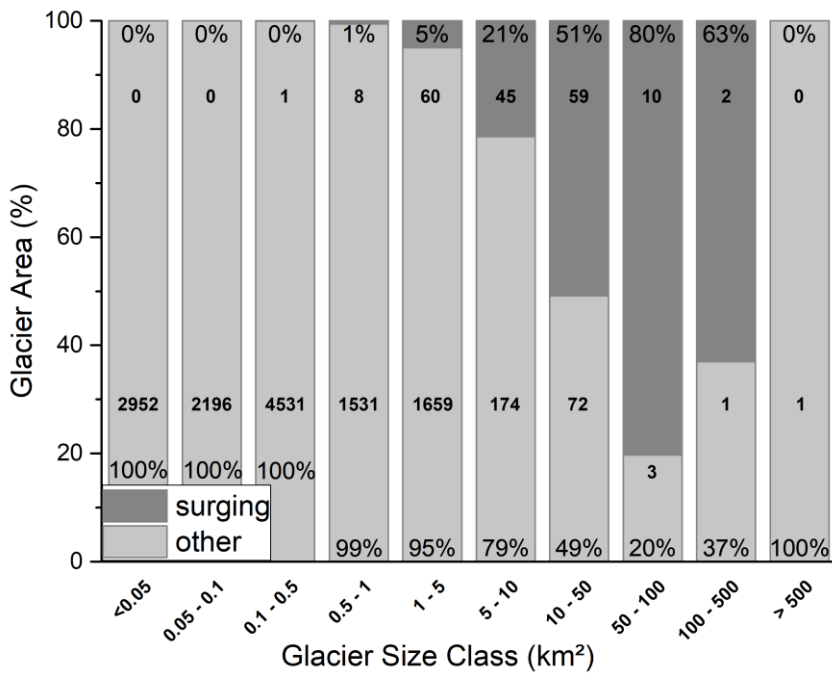
777



778

779 Fig. 6: Overview of the identified surging glaciers (red) in the Pamir Mountains. Small black numbers refer to
 780 their ObjectID in the GI-3min dataset, numbers in circles indicate glaciers mentioned in the text and bold white
 781 numbers indicate regions mentioned in the text (1 Petr Alervogo West, 2 Petr Alervogo East, 3 Fedchenko, 4
 782 King Tau, 5 Ulugartag, 6 Mustagh). DEM source: AW3D30.

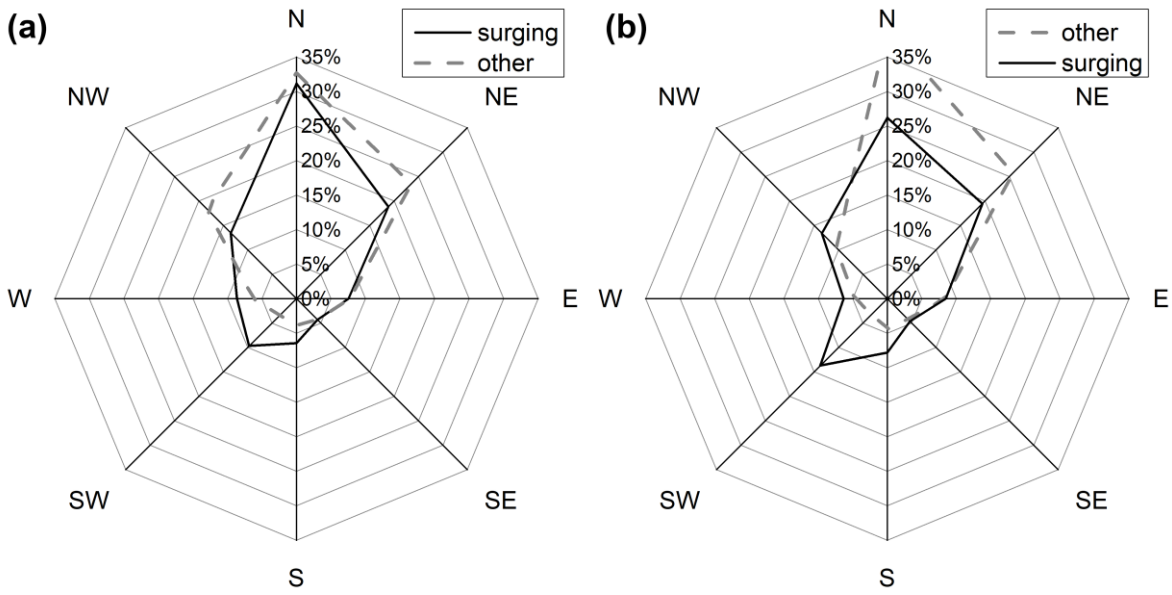
783



784

785 Fig. 7: Size class distribution (in relative terms) of surging and other glaciers in GI-2. The upper bold numbers
 786 provide the count for surge glaciers, the lower one for all other glaciers.

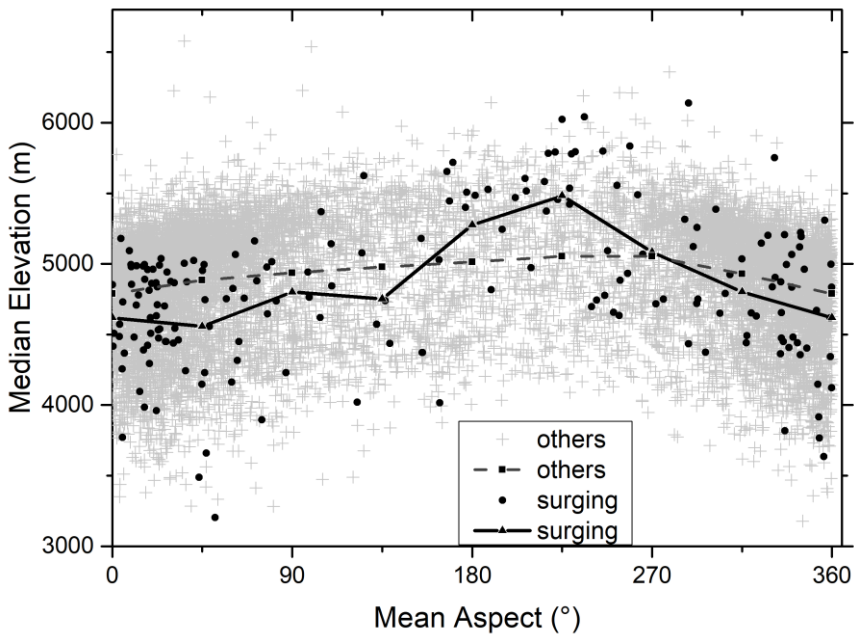
787



788

789 *Fig. 8: Aspect sector distribution for surging and other glaciers (in relative terms) per a) count and b) area*
 790 *covered.*

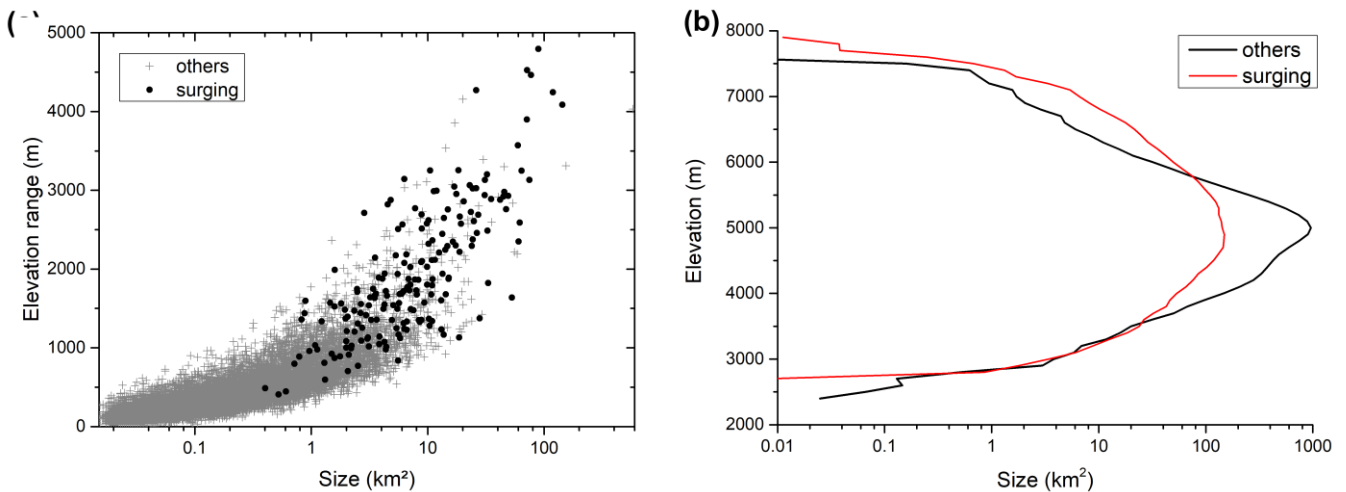
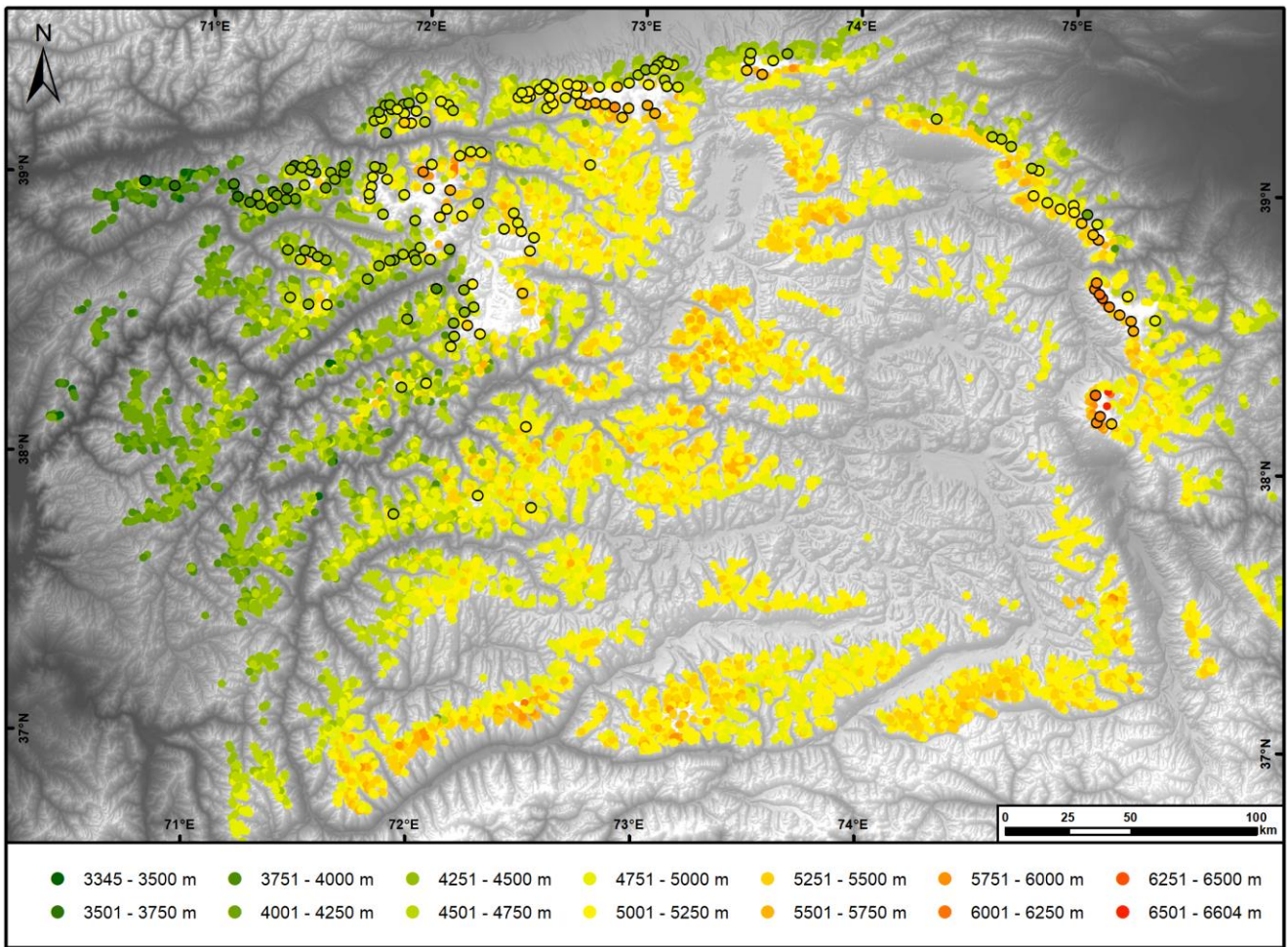
791

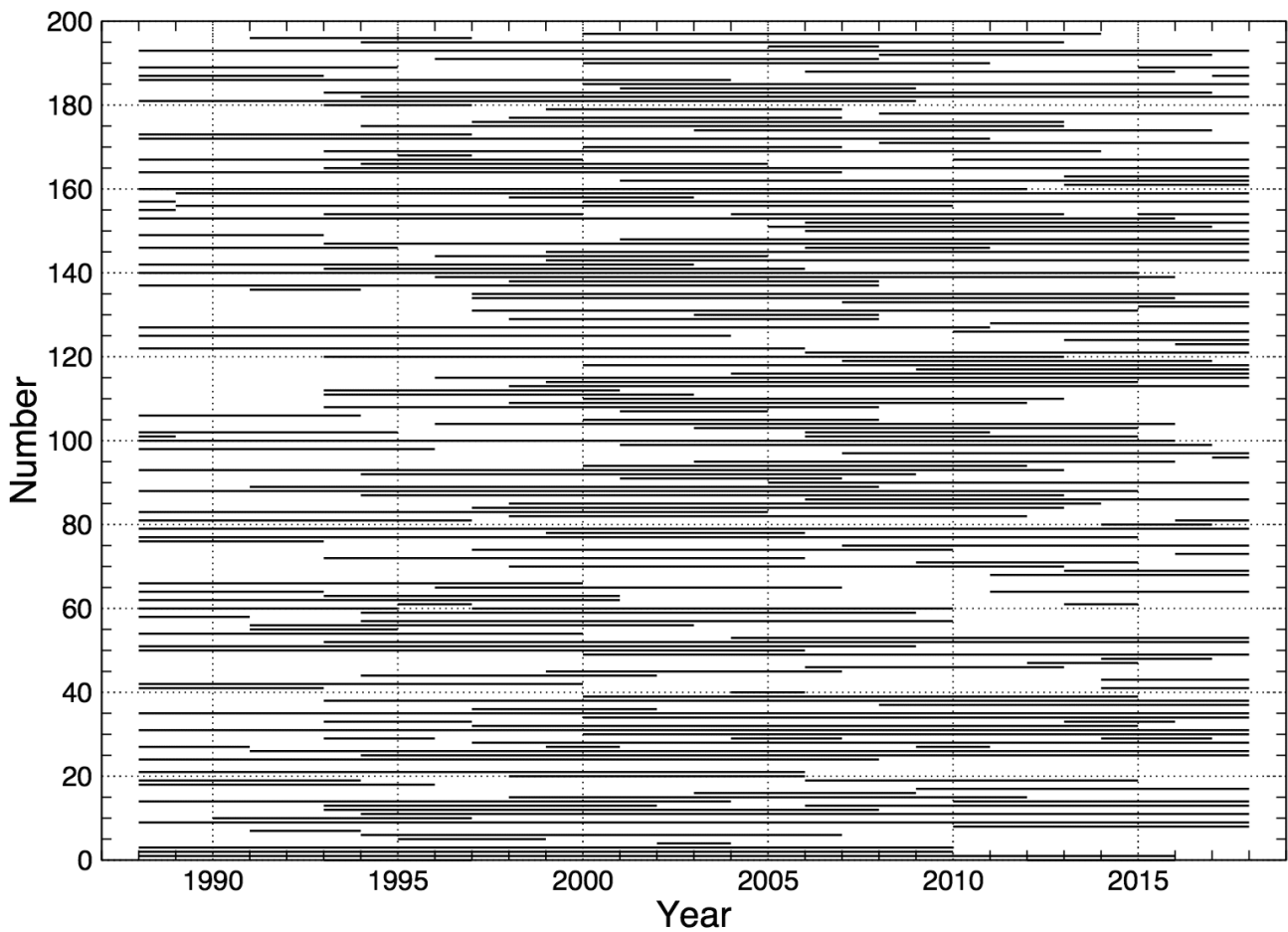


792

793 *Fig. 9: Mean aspect vs. median glacier elevation for surging and other glaciers. The connected lines are*
 794 *averages per aspect sector.*

795

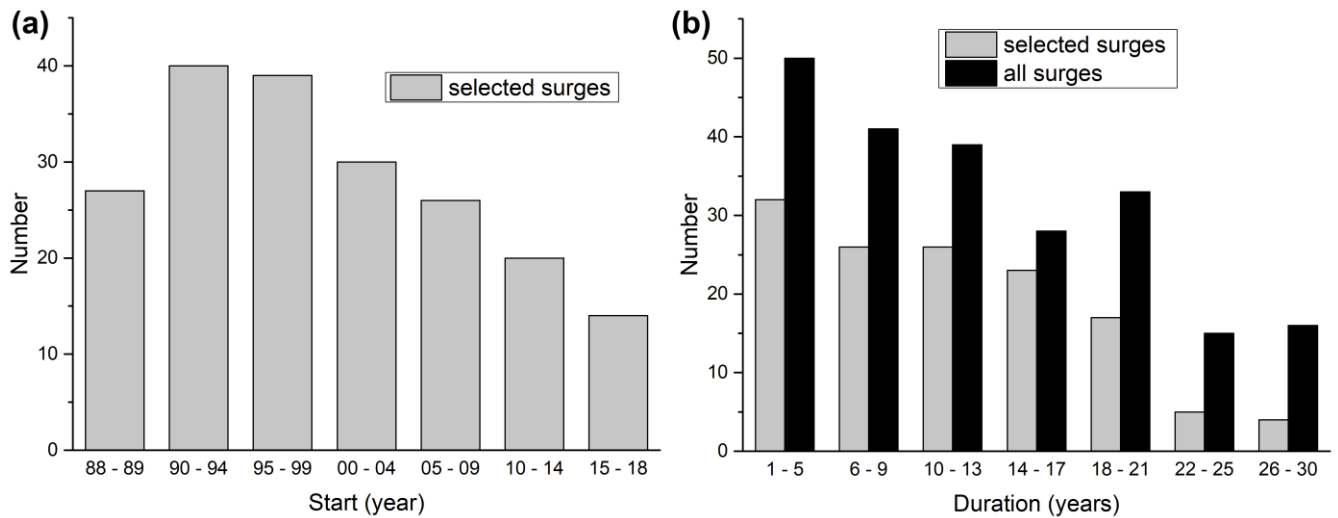




804

805 *Fig. 12: Surge periods for all glaciers with observed surges (GI-3min). Those starting (ending) in 1988 (2018)*
 806 *might have started earlier / last longer than indicated by the line.*

807



808

809 *Fig. 13: Histograms of surge characteristics. a) Periods in which the surges have started, b) surge durations. The*
 810 *charts provide greater detail than the classification code to allow for a better analysis and keep the glacier code*
 811 *in the inventory simple. The “88-89” label in a) includes only glaciers that started surging in 1989 as we cannot*
 812 *be sure about a surge start of 1988 (might also been earlier). The grey bars in b) refer to the surges that*
 813 *occurred completely within the study period, i.e. started after 1988 and ended before 2018.*

814

815